Optics Letters

Characterization of spatiotemporal chaos in a Kerr optical frequency comb and in all fiber cavities

Z. Liu,[1] M. Ouali,[1] S. Coulibaly,[1,*] M. G. Clerc,[2] M. Taki,[1] and M. Tlidi[3]

[1]Université de Lille, CNRS, UMR 8523-PhLAM-Physique des Lasers Atomes et Molécules, F-59000 Lille, France
[2]Departamento de Física, FCFM, Universidad de Chile, Casilla 487-3, Santiago, Chile
[3]Optique Nonlinéaire Théorique, Université Libre de Bruxelles (U.L.B.), CP 231, Campus Plaine, B-1050 Bruxelles, Belgium
*Corresponding author: saliya.coulibaly@univ-lille1.fr

Received 28 December 2016; revised 10 February 2017; accepted 13 February 2017; posted 14 February 2017 (Doc. ID 283776); published 3 March 2017

Complex spatiotemporal dynamics have been a subject of recent experimental investigations in optical frequency comb microresonators and in driven fiber cavities with Kerr-type media. We show that this complex behavior has a spatiotemporal chaotic nature. We determine numerically the Lyapunov spectra, allowing us to characterize different dynamical behavior occurring in these simple devices. The Yorke–Kaplan dimension is used as an order parameter to characterize the bifurcation diagram. We identify a wide regime of parameters where the system exhibits a coexistence between the spatiotemporal chaos, the oscillatory localized structure, and the homogeneous steady state. The destabilization of an oscillatory localized state through radiation of counter-propagating fronts between the homogeneous and the spatiotemporal chaotic states is analyzed. To characterize better the spatiotemporal chaos, we estimate the front speed as a function of the pump intensity.

OCIS codes: (070.5753) Resonators; (190.4370) Nonlinear optics, fibers; (190.3100) Instabilities and chaos; (190.5530) Pulse propagation and temporal solitons.

https://doi.org/10.1364/OL.42.001063

Experiments supported by numerical simulations of driven cavities such as whispering-gallery-mode microresonators leading to optical frequency comb generation have demonstrated the existence of complex spatiotemporal dynamics [1]. Similar complex dynamics have been observed in all-fiber cavities [2–4]. In most of these studies, complex behaviors are characterized by a power spectrum [1], filtering spatiotemporal diagrams [4], embedding dimension, and time series analysis [2,3]. However, these tools are inadequate to distinguish between spatiotemporal chaos, low dimensional chaos, and turbulence. A classification of these phenomena has been reported in the literature (see for instance [5–11]). In the case of spatiotemporal chaos, the Lyapunov spectrum has a continuous set of positive values. This matches the definition that has been proposed in [5,7]. In the case of a low dimensional chaos, the Lyapunov spectrum possesses a discrete set of positive values. However, the turbulence or weak turbulence is characterized by a power law cascade of a scalar quantity such as energy and norm [12]. On the basis of the Lyapunov spectrum, we cannot conclude that the system develops a turbulence.

In this Letter, we characterize the complex behavior reported in the paradigmatic Lugiato–Lefever equation (LLE, [13]) that describes Kerr optical frequency combs and fiber cavities. For this purpose, we use a rigorous tools of dynamical systems theory. We show that this complex behavior has a spatiotemporal chaotic nature. We estimate the Lyapunov spectra. The Yorke–Kaplan dimension (D_{YK}) is used as an order parameter to establish the bifurcation diagram of the spatiotemporal chaos. In addition, we show that the spatiotemporal chaos, the oscillatory localized state and the homogeneous steady state (HSS) can coexist in a finite range of the pumping intensity. The destabilization of an oscillatory localized state through radiation of counter-propagating fronts between the HSS and the spatiotemporal chaotic state is also discussed by estimating the front speed as a function of the pump intensity.

Driven Kerr cavities with a high Fresnel number—assuming that the cavity is much shorter than the diffraction and the nonlinearity spatial scales—is described in the mean field limit by the LLE [13]. This equation has been extended to model both fiber cavities [14,15] and optical frequency comb generation [16–18], in which the diffraction is replaced by dispersion. This model reads

$$\frac{\partial \psi}{\partial t} = S - (\alpha + i\delta)\psi + \frac{i}{2}\frac{\partial^2 \psi}{\partial \tau^2} + i|\psi|^2\psi, \tag{1}$$

where $\psi(t,\tau)$ is the normalized slowly varying envelope of the electric field that circulates within the cavity, and S is the amplitude of the injected field which is real and constant. The time variable t corresponds to the slow evolution of ψ over successive round-trips. τ accounts for the fast dynamics that describes how the electric field envelope changes along the fiber [14–16]. The parameters α and δ are the cavity losses,

and the cavity detuning, respectively. In addition, Eq. (1) has been derived in the context of left-handed materials [19]. Note that Eq. (1) has been derived in early reports to describe the plasma driven by a radio frequency field [20,21] and the condensate in the presence of an applied ac field [22].

The model, Eq. (1), supports stationary localized [23] and self-pulsating localized [24] structures. In the conservative limit, $(\alpha, S) \to (0, 0)$, localized structures have analytical solutions [25–28]. It has been also shown that, in this limit, localized structures can exhibit regular time oscillations and display a complex behavior [25–27]. An example of complex spatiotemporal behavior is plotted in the $\tau - t$ map of Fig. 1(a). The time evolution of the field amplitude that circulates inside the cavity exhibits large amplitude localized pulses. These pulses have irregular distribution along the τ coordinate [see Fig. 1(a)]. The characterization of this behavior can be achieved by means of Lyapunov exponents, which provide an information about the sensitivity of close initial conditions [7]. When the largest Lyapunov exponent is positive, the system develops chaos, but not necessarily a spatiotemporal chaos. To distinguish between these two complex dynamical behaviors, it is necessary to compute the Lyapunov spectra composed by a set of exponents [5–7]. Spatiotemporal chaos has a Lyapunov spectrum with a *continuous* set of positive values. In contrast, chaos possesses a Lyapunov spectrum with a discrete set of positive values. The Lyapunov exponents is denoted by $\{\lambda_i\}$, where i labels the exponents ($i = 1, \ldots, N$) and $\lambda_p \leq \lambda_q$ ($p \geq q$). By using the strategy proposed in [29,30], we compute numerically the Lyapunov spectrum for large N. The numerical simulations are obtained by using periodic boundary conditions that are compatible with both Kerr optical frequency combs and fiber cavity geometries. Figure 1(b) shows a typical continuous Lyapunov spectrum. Hence, we infer that the complex dynamical behavior shown in Fig. 1(a) is a spatiotemporal chaos.

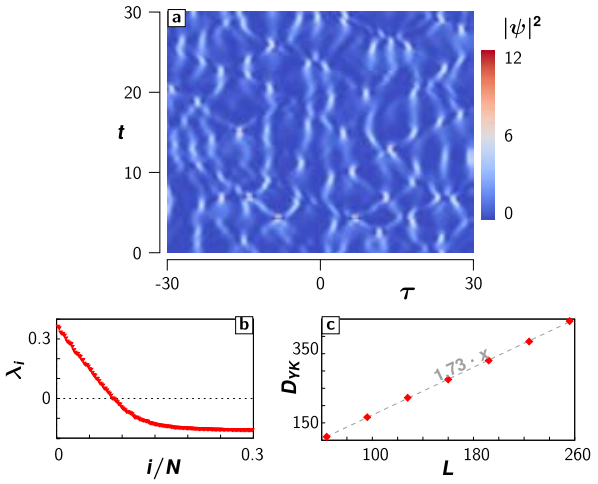

Fig. 1. Spatiotemporal chaos. (a) $\tau - t$ map shows a complex spatiotemporal behavior obtained by numerical simulation of Eq. (1) with $\alpha = 0.16$, $\delta = 1$, and $S^2 = 0.16$ with 512 grid points. (b) Corresponding Lyapunov spectrum, and (c) Yorke–Kaplan dimension as a function of the system size L is indicated by the diamond red points. $L = 512\Delta\tau$ with $\Delta\tau$ is the step-size integration. The linear growth of D_{YK} dimension is fitted by a slope of 1.73, as shown by the gray dashed line.

The main feature of the Lyapunov spectra is that they are proportional to the physical system size. This implies that the upper limit of the strange attractor dimension of spatiotemporal chaos—the Kaplan–Yorke dimension (D_{YK})—is an extensive quantity that increases with the physical system size [6]. This latter quantity provides an information on the level of the strange attractor complexity and is defined by [31]

$$D_{YK} \equiv p + \frac{\sum_{i=1}^{p} \lambda_i}{\lambda_{p+1}}, \tag{2}$$

where p is the largest integer that satisfies $\sum_{i=1}^{p} \lambda_i > 0$. Figure 1(c) displays D_{YK} as a function of the number of discretization points, which shows that this dimension is indeed an extensive physical quantity as it linearly increases with the system size. Therefore, as one increases the system size, the dimension of the strange attractor grows proportionally.

To establish the bifurcation diagram of the spatiotemporal chaos, we fix the detuning and the dissipation values, and we numerically estimate D_{YK} by varying the pumping intensity. The initial condition consists of a single peak localized structure. The summary of the results is illustrated in Fig. 2. When increasing the pump intensity, the LLE has a zero Yorke–Kaplan dimension, i.e., $D_{YK} = 0$ until the system reaches $S^2 \equiv S_+^2$. For $S^2 > S_+^2$, the system exhibits a transition toward a spatiotemporal chaos, i.e., $D_{YK} > 0$. This behavior lasts for large pumping intensity values. When decreasing S^2, the spatiotemporal chaos persists down to the point $S^2 \equiv S_-^2$, as shown in Fig. 2. From this figure, we clearly see a hysteresis loop involving a spatiotemporal chaos, a pulsating localized structure, and a HSS in the range $S_-^2 < S^2 < S_+^2$. The inset in Fig. 2 shows the continuous Lyapunov spectra for different values of the pump intensity. Remarkably, the middle panel of the inset shows two Lyapunov spectra (Γ_2 and Γ_3) obtained for the same parameters values indicating the coexistence of two qualitatively different dynamical behaviors.

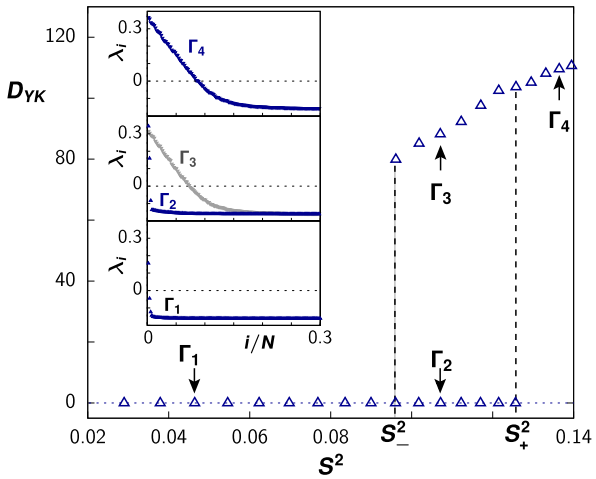

Fig. 2. Bifurcation diagram of spatiotemporal chaos showing the Yorke–Kaplan dimension, D_{YK}, as a function of the intensity of pumping obtained by numerical simulations of Eq. (1). The insets account for the Lyapunov spectra obtained for four values of the pumping intensity indicated by the symbol Γ_j ($j = 1, 2, 3, 4$). The parameters are $\delta = 1$, and $\alpha = 0.16$. The grid points is 512. The spectra are composed of $N = 496$ exponents.

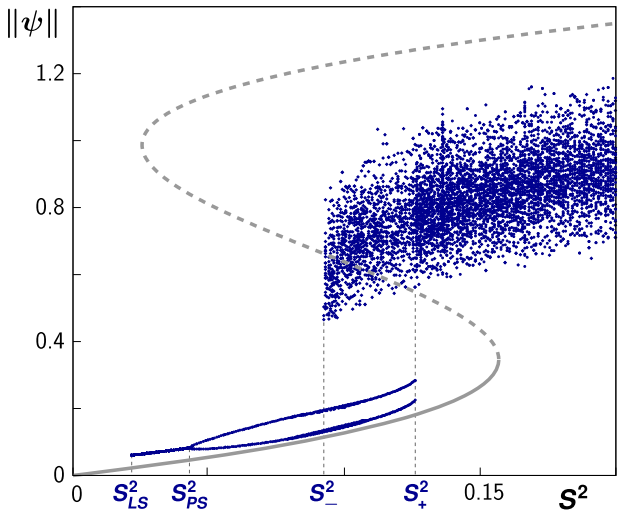

Fig. 3. Bifurcation diagram of model Eq. (1). The total intracavity intensity $\|\psi\|$ versus the pump intensity S^2 with $\delta = 1$, and $\alpha = 0.16$. The continuous and dashed thick gray lines point out the stable and unstable HSS, respectively. The continuous blue lines indicate the extrema of the total intracavity intensity $\|\psi\|$ of localized states. The cloud of blue scattered points accounts for the spatiotemporal chaotic state. Note that the horizontal graduation unit is equal to 0.05.

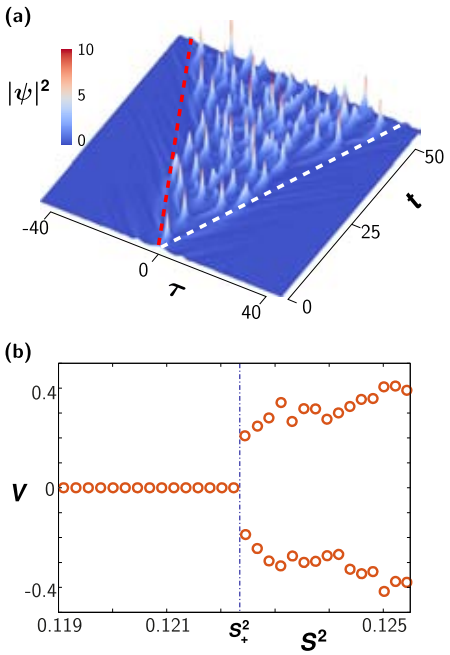

Fig. 4. Front radiation from an oscillating unstable localized state. (a) Spatiotemporal evolution of oscillatory localized structures obtained from the numerical simulation of Eq. (1). The parameters are $S^2 = 0.1225$, $\delta = 1$, and $\alpha = 0.16$. The dashed lines mark a separation between the chaotic and the homogeneous background. From these lines, one can determine the front speed. (b) Front speed V as a function of the pump intensity obtained for $\delta = 1$ and $\alpha = 0.16$.

In what follows, we establish a bifurcation diagram showing a coexistence between the spatiotemporal chaos, the oscillatory localized structure, and the HSS. In order to show different operating regimes, the total intracavity field amplitude $\|\psi\| \equiv \int |\psi(t,\tau)|^2 d\tau$ as a function of the pumping intensity is shown in the bifurcation diagram Fig. 3. The upper (lower) HSS branch indicated by a dashed (solid) gray line is modulationally unstable (stable) [13]. For small pumping intensity, the system has a stationary stable localized state in the range $S^2_{\mathrm{LS}} < S^2 < S^2_{\mathrm{PS}}$ (see Fig. 3). When increasing the pumping intensity, the localized state becomes self-pulsating in the range $S^2_{\mathrm{PS}} \le S^2 < S^2_+$. When further increasing S^2, the system exhibits spatiotemporal chaos. When decreasing S^2, the spatiotemporal chaos persists down to S^2_-. As in the bifurcation diagram of D_{YK} (see Fig. 2), the system presents an hysteresis loop involving three different robust states: HSS, pulsating localized structures, and spatiotemporal chaos.

It is well known that model (1) exhibits radiation from a localized state of two counter-propagating fronts between the homogeneous and the complex spatiotemporal states [32]. An example of this behavior is depicted in the $\tau - t$ map shown in Fig. 4(a). To characterize this transition, we estimate numerically the front speed. Figure 4(b) shows the front speed as a function of the pump intensity in the vicinity of the instability associated with localized states. Right and left fronts propagate with almost the same speed. As the pumping intensity is increased, the front speed continues to increase until the system reaches the lower limit point of bistable HSSs. Similar behavior has been reported in pattern forming systems where the front propagates between a HSS and a periodic pattern [33–35], between either of the two HSSs [36,37], or even between a HSS and the spatiotemporal intermittency [38].

From a practical point of view, a driven ring cavity made with an optical fiber could support a spatiotemporal regime. However, by using a constant injected beam, i.e., cw operation, it is hard to reach the high-intensity regime where we can observe the spatiotemporal chaos and its coexistence with a homogeneous background. To overcome this limitation, it is necessary to drive the cavity by synchronously pumping with a pulsed laser. The time-of-flight of the light pulses in the cavity should be adjusted to the laser repetition time. All experiments using this simple device with a pulse laser have shown evidence of complex spatiotemporal behaviors [2–4,39]. Therefore, the phenomenon described in this Letter should be observed experimentally.

In conclusion, by using rigorous tools of dynamical system theory, such as Lyapunov spectra, we have quantitatively shown that the complex behavior observed experimentally in the Kerr optical frequency combs [1] and in the fiber cavity [2–4] is of a spatiotemporal chaos nature. We have also shown that the Yorke–Kaplan dimension can be considered as a good order parameter to characterize the bifurcation diagram associated with spatiotemporal chaos. Finally, we have identified different operating regimes, in particular the coexistence between spatiotemporal chaos, the self-pulsating localized structure, and the homogeneous steady state. The observed complex states are exponentially sensitive to the initial conditions, exhibit complex spatiotemporal chaos, and have exponential power spectrum. Hence, this behavior is not of a turbulent nature. Therefore, our finding is important for the analysis, or classification of the various complex spatiotemporal behaviors observed in practical dissipative systems.

Funding. FONDECYT (1150507); Belgian Science Policy Office Interuniversity Attraction Poles (IAP P7-35 «photonics@be»); ANR Blanc OptiRoc (N12-BS04-0011); Laboratoire d'Excellence: Centre Européen pour les Mathématiques, la Physique et leurs Interactions; Fonds National de la Recherche Scientifique.

Acknowledgment. M. G. Clerc is grateful to the financial support of FONDECYT projects 1150507. Z. Liu, S. Coulibaly, and M. Taki are grateful to the Interuniversity Attraction Poles program of the Belgian Science Policy Office under the grant IAP P7-35 «photonics@be», the French Project ANR Blanc OptiRoc N12-BS04-0011, and the "Laboratoire d'Excellence: Centre Européen pour les Mathématiques, la Physique et leurs Interactions" CEMPI. M. Tlidi received support from the Fonds National de la Recherche Scientifique (Belgium).

REFERENCES

1. Y. K. Chembo, D. V. Strekalov, and N. Yu, Phys. Rev. Lett. **104**, 103902 (2010).
2. F. Mitschke, G. Steinmeyer, and A. Schwache, Physica D **96**, 251 (1996).
3. G. Steinmeyer, A. Schwache, and F. Mitschke, Phys. Rev. E **53**, 5399 (1996).
4. M. Anderson, F. Leo, S. Coen, M. Erkintalo, and S. G. Murdoch, Optica **3**, 1071 (2016).
5. P. Manneville, *Dissipative Structures and Weak Turbulence* (Academic, 1990).
6. D. Ruelle, Commun. Math. Phys. **87**, 287 (1982).
7. A. Pikovsky and A. Politi, *Lyapunov Exponents: A Tool to Explore Complex Dynamics* (Cambridge University, 2016).
8. G. Nicolis, *Introduction to Nonlinear Science* (Cambridge University, 1995).
9. M. G. Clerc and N. Verschueren, Phys. Rev. E **88**, 052916 (2013).
10. F. Selmi, S. Coulibaly, Z. Loghmari, I. Sagnes, G. Beaudoin, M. G. Clerc, and S. Barbay, Phys. Rev. Lett. **116**, 013901 (2016).
11. S. Coulibaly, M. G. Clerc, F. Selmi, and S. Barbay, Phys. Rev. A **95**, 023816 (2017).
12. U. Frisch, *Turbulence: The Legacy of AN Kolmogorov* (Cambridge University, 1995).
13. L. A. Lugiato and R. Lefever, Phys. Rev. Lett. **58**, 2209 (1987).
14. M. Haelterman, S. Trillo, and S. Wabnitz, Opt. Commun. **91**, 401 (1992).
15. M. Haelterman, S. Trillo, and S. Wabnitz, Opt. Lett. **17**, 745 (1992).
16. Y. K. Chembo and C. R. Menyuk, Phys. Rev. A **87**, 053852 (2013).
17. T. Hansson, D. Modotto, and S. Wabnitz, Phys. Rev. A **88**, 023819 (2013).
18. A. Coillet, J. Dudley, G. Genty, L. Larger, and Y. K. Chembo, Phys. Rev. A **89**, 013835 (2014).
19. P. Kockaert, P. Tassin, G. Van der Sande, I. Veretennicoff, and M. Tlidi, Phys. Rev. A **74**, 033822 (2006).
20. G. J. Morales and Y. C. Lee, Phys. Rev. Lett. **33**, 1016 (1974).
21. K. Nozaki and N. Bekki, Phys. Lett. A **102**, 383 (1984).
22. D. J. Kaup and A. C. Newell, Phys. Rev. **18**, 5162 (1978).
23. A. J. Scorggie, W. J. Firth, G. S. McDonald, M. Tlidi, R. Lefever, and L. A. Lugiato, Chaos Solitons Fractals **4**, 1323 (1994).
24. D. Turaev, A. G. Vladimirov, and S. Zelik, Phys. Rev. Lett. **108**, 263906 (2012).
25. K. Nozaki and N. Bekki, J. Phys. Soc. Jpn. **54**, 2363 (1985).
26. K. Nozaki and N. Bekki, Physica D **21**, 381 (1986).
27. M. Taki, K. H. Spatschek, J. C. Fernandez, and R. Grauer, Physica D **40**, 65 (1989).
28. S. Wabnitz, Opt. Lett. **18**, 601 (1993).
29. F. Christianen and H. H. Rough, Nonlinearity **10**, 1063 (1997).
30. T. J. Bridges and S. Reich, Physica D **156**, 219 (2001).
31. E. Ott, *Chaos in Dynamical Systems*, 2nd ed. (Cambridge University, 2002).
32. F. Leo, L. Gelens, P. Emplit, M. Haelterman, and S. Coen, Opt. Express **21**, 9180 (2013).
33. Y. Pomeau, Physica D **23**, 3 (1986).
34. M. G. Clerc, C. Falcon, and E. Tirapegui, Phys. Rev. Lett. **94**, 148302 (2005).
35. M. G. Clerc, C. Falcon, and E. Tirapegui, Phys. Rev. E **74**, 011303 (2006).
36. S. Coen, M. Tlidi, Ph. Emplit, and M. Haelterman, Phys. Rev. Lett. **83**, 2328 (1999).
37. S. Coulibaly, M. Taki, and M. Tlidi, Opt. Express **22**, 483 (2014).
38. M. G. Clerc, S. Coulibaly, M. Ferré, M. A. García-Ñustes, and R. G. Rojas, Phys. Rev. E **93**, 052204 (2016).
39. F. Mitschke and A. Schwache, J. Opt. B **10**, 779 (1998).